JOURNAL OF SPACECRAFT AND ROCKETS
Vol. 48, No. 2, March–April 2011

Drag Coefficients of Satellites with Concave Geometries: Comparing Models and Observations

Marcin D. Pilinski,* Brian M. Argrow,† and Scott E. Palo‡
University of Colorado, Boulder, Colorado 80309

DOI: 10.2514/1.50915

Predictions of satellite orbital perturbations often contain uncertainties due to the use of constant drag coefficients. While convex satellites may be analyzed using analytical solutions, concave geometry must be treated numerically, taking into account the effects of secondary reflections and flow shadowing. To evaluate these effects, the direct simulation Monte Carlo method was compared with analytical convex-shaped equations in free molecular flow with the measured drag of Starshine I, II, and III. The Starshine satellites were covered by hundreds of small mirrors, resulting in varying degrees of surface concavity. Ballistic coefficient measurements were collected by the United States Air Force Space Command and are adjusted herein for atmospheric model biases as well as new estimates of the Starshine cross-sectional areas. The addition of the mirrors was analyzed using two approaches. The first approach assumed that molecules were successively accommodated with each surface impact. The second method assumed that a molecule accommodates most during its first surface impact. The second model predicted an increase in the drag coefficients of concave objects, which is in agreement with drag observations of smooth and rough spherical satellites. The results indicate a 7–25% correction to the drag force and ballistic coefficient of the Starshine satellites.

Nomenclature

A	=	projected area, m^2
A_p	=	planetary geomagnetic index
a, b	=	empirical leak rate coefficients
B	=	ballistic coefficient, $m^2\ kg^{-1}$
C_D	=	drag coefficient
d	=	average molecular diameter, m
E	=	kinetic energy, eV
F	=	force, N
FC	=	fraction of molecules leaving the surface after n reflections
$F10.7$	=	solar flux of 10.7 cm wavelength radiation, solar flux units
f	=	fraction of molecules undergoing at least n reflections
K_N	=	Knudsen number
k_b	=	Boltzmann constant, $m^2\ kg\ s^{-2}\ K^{-1}$
L	=	characteristic length, m
M	=	spacecraft mass, kg
m	=	molecular mass, kg
n	=	number density, m^{-3}
s	=	speed ratio
T	=	temperature, K
V	=	velocity magnitude, m/s
$\mathbf{V}$	=	velocity vector, m/s
$\mathbf{v}$	=	velocity direction unit vector
α	=	energy accommodation coefficient
β	=	reciprocal of the most probable speed, s/m
θ	=	pitch angle, deg
λ	=	mean free path, m
ρ	=	mass density, $kg\ m^{-3}$

Subscripts

aw	=	atmospheric wind
i	=	incoming (freestream) molecules
k	=	kinetic
j	=	atmospheric species index
max	=	maximum of area distribution
min	=	minimum of area distribution
mode	=	mode of area distribution
n	=	nth reflection
r	=	reflected molecules
sc	=	spacecraft
T	=	total (spacecraft + wind)
w	=	wall conditions

Received 25 May 2010; revision received 10 August 2010; accepted for publication 15 August 2010.

*Graduate Research Assistant, Department of Aerospace Engineering Sciences.

†Associate Fellow, Professor of the Department of Aerospace Engineering Sciences, Director of Research and Engineering Center for Unmanned Vehicles.

‡Associate Professor, Department of Aerospace Engineering Sciences, Colorado Center for Astrodynamics Research, Research and Engineering Center for Unmanned Vehicles.

Introduction

AERONOMIC studies make use of satellite drag measurements in the determination of thermospheric densities, enabling scientific inquiry into processes of the upper neutral atmosphere. There is also significant work applied to the inverse problem of predicting satellite drag based on atmospheric density models. The goals of improving drag coefficient and density modeling are motivated by increasing orbit-prediction accuracy for applications such as reentry forecasts, improving the accuracy of orbit determination, and increasing our understanding of planetary atmospheres. To form an accurate solution in any of these cases, forces on the satellite in the direction of flight must be correctly related to the density of the atmosphere. The core of this relation is the drag coefficient C_D, which is a function of satellite geometry, the atmospheric gas properties, and the manner in which the gas and surface interact physically. It is important to distinguish the physical definition just given from that used in statistical orbit determination, wherein the drag coefficient is one of the parameters adjusted to make the observed orbit match the modeled predictions. This fitted drag coefficient includes unmodeled density signals along with other orbit propagation errors. While there are analytical solutions [1–3] to the physical drag coefficient, the assumptions inherent in many of these techniques do not allow for the treatment of concave surfaces where, due to the geometry, a single molecule may undergo many reflections

with the surface. A numerical scheme is needed in order to adequately describe the interactions of molecules with such geometry.

The purpose of this work is to compare analytical and numerical solutions to the observed drag coefficients of several satellites at various altitudes to determine which modeling technique is most accurate. Specifically, we will focus on cases where the measured drag coefficients disagree significantly with analytical predictions and evaluate several numerical schemes and gas–surface assumptions for computing the drag coefficient to determine if they can reduce or eliminate the discrepancy. The numerical schemes to be examined include a direct simulation Monte Carlo (DSMC) approach developed by Bird [4] as well as a test particle Monte Carlo technique described by Davis [5] and implemented by the authors. Model solutions will also be compared with analytical approximations. The analysis is focused on the drag coefficient of Starshines I, II, and III [6,7] due to their varying degrees of surface concavity and the difficulty that their drag coefficients have presented to previous attempts at analytic solution [8]. Drag coefficient observations were determined by the U. S. Air Force Space Command Space Analysis Office through tracking of satellite orbits, solving for the drag forces, and comparing these against a calibrated atmospheric density model [9].

In their previous analysis of Starshine drag coefficients, Bowman and Moe [10] concluded that the drag of these modified spheres is significantly greater than that of regular spheres. We will show here that most of this discrepancy in the Starshine drag coefficients is due to the use of a cross-sectional area based on a sphere rather than the true satellite geometry. This correction to the cross section and the corresponding adjustment to the ballistic coefficient has a significant effect on the atmospheric densities derived from the orbital perturbations of these objects [11–13]. Both the reanalysis of Starshine data as well as numerical models applied to high-fidelity representation of the Starshine surfaces indicate that the concave features cause the drag coefficient of these objects to be higher than that of a sphere. The same previous study by Bowman and Moe [10] found the observed drag coefficient of a sandblasted sphere is higher than that of a polished sphere, which is in agreement with our finding that surface irregularities can raise drag in the free molecular regime.

Physics of Drag Coefficients

Equations (1) and (2) describe the aerodynamic drag force experienced by a spacecraft in free molecular flow (FMF). In general, spacecraft experience lift in both the orbit-normal and orbit-radial directions due to interaction with the atmosphere. In our consideration of near-spherical objects, we will restrict our analysis only to the drag force. As previously stated, the atmospheric drag force on satellites is a direct function of drag coefficient C_D. Errors in this parameter contribute directly to the fidelity of density measurements. The same is true of the cross-sectional area and spacecraft mass, as seen in Eqs. (1) and (2). Cross-sectional area computation, though not as involved as drag coefficient estimation, is not a trivial process if the satellite attitude is changing in unknown ways or if the exact spacecraft geometry is unknown. We will return to the computation of cross-sectional area:

$$\mathbf{F} = \tfrac{1}{2}A \cdot C_D \cdot \rho \cdot \|\mathbf{V}_{\text{aw}} - \mathbf{V}_{\text{sc}}\|^2(-\mathbf{v}_T) \tag{1}$$

$$-\mathbf{v}_T = \frac{(\mathbf{V}_{\text{aw}} - \mathbf{V}_{\text{sc}})}{\|\mathbf{V}_{\text{aw}} - \mathbf{V}_{\text{sc}}\|} \tag{2}$$

In the previous equations, $\mathbf{F}$ is the drag force vector (kg m s^{-2}), A is the projected area of the object (m^2), C_D is the unitless coefficient of drag, ρ is the mass density (kg/m^3), and $\mathbf{V}_{\text{aw}}$ and $\mathbf{V}_{\text{sc}}$ are the atmospheric wind and the spacecraft velocity vectors (m/s), respectively. The relative orientation of drag acceleration and spacecraft motion is shown in Fig. 1 for a spherically symmetric object. Although the mass and cross-sectional area may be determined a priori, the drag coefficient is a function of many parameters, including gas–surface interactions, satellite surface contamination,

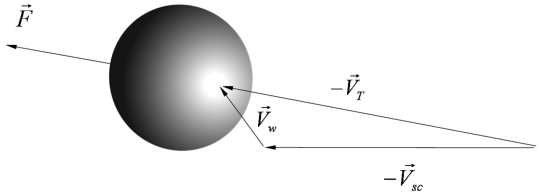

Fig. 1 Vector variables of the drag equation.

and atmospheric composition [14], and its estimation has proved a challenge to scientists and engineers studying the atmosphere. These parameters are functions of solar activity, altitude, season, and geomagnetic location, among other things, so it is a simplification to write the drag coefficient as a function of altitude and solar activity only. One example of the consequence drag coefficient estimation can have on modeling is the introduction of density biases in atmospheric density models. Cook [15] computed an appropriate drag coefficient for satellites of various shapes that could be applied for all altitudes and atmospheric conditions. At the time of his derivation, the problem of drag coefficient variability was indeterminate and using a constant value was the best choice. We now have a better understanding of how the drag coefficient varies with atmospheric properties [16] and how the results of using constant C_D in the determination of atmospheric density are altitude-dependent biases in the density models [10].

To decouple the product of drag coefficient and density, a physically appropriate estimate of the coefficient must be made and must take into account the effects of gas–surface accommodation, usually written as a coefficient that is a measure of the relative amount of kinetic energy molecules lose during reflection from the satellite surface. Much like reflectivity in optics, the accommodation coefficient α is treated as an empirical parameter effective over the entire satellite surface. Momentum and its time rate of change (force) are particularly sensitive to accommodation, and it has been postulated [17] that in low Earth orbit (LEO), α is strongly related to atomic oxygen adsorption on the satellite surface. Thus, the altitude dependence of the drag coefficient is driven by changes in the quantity of atomic oxygen surface adsorption, which indicates that changes in atmospheric density can also lead to changes in a satellite's drag coefficient. The exact physical process behind this variation is uncertain, but empirical data exist for the energy accommodation coefficient as a function of altitude based on some limited measurements [8,18]. The accommodation coefficient α is formally defined as [19]

$$\alpha = \frac{T_{k,i} - T_{k,r}}{T_{k,i} - T_w} \tag{3}$$

where $T_{k,i}$ is the kinetic temperature carried to the surface by an incoming molecule, $T_{k,r}$ is the temperature of the reflected molecule, and T_w is the temperature the molecule would have if it was reemitted at the temperature of the surface [3]. Kinetic temperature can be written as [3]

$$T_{k,i} = \frac{mV_T^2}{3k_b} \tag{4}$$

where V_T is the magnitude of incident velocity, and k_b is the Boltzmann constant. The reflected kinetic temperature at the surface is defined as

$$T_{k,r} = \frac{m}{3k_b} V_T^2(1 - \alpha) + \alpha T_w \tag{5}$$

Equation (4) only applies to monatomic molecules. The error in drag coefficient introduced by treating molecular nitrogen, using Eqs. (4) and (5), is estimated to be less than 1%. In general, two types of reflection are ascribed to gas–surface interactions in LEO [17,20,21]. The majority of interactions below 500 km [17] are diffuse in character with a scattering kernel, first described by Maxwell [22], where the velocities of reflected molecules are

centered around the surface normal vector in a cosine distribution. The second type is quasi-specular reflection, where the molecules are reflected in a narrow lobe that is centered around the specular direction. When computing the drag coefficient, a successful technique [14] is the adaptation of the drag coefficient models of Sentman (diffuse) [1] and Schamberg (quasi specular) [2] with the use of empirical accommodation coefficient profiles for the former and Goodman's model of accommodation [23] for the latter. Sentman's model [1] adapts the diffuse (or Maxwellian) energy distribution with a variable accommodation coefficient. The quasi-specular version of Schamberg's model [2] reflects the majority of molecules around a direction, such that the angle of reflection (as defined from the surface) is slightly larger or equal to the incident angle. These reflection models are visually presented in Fig. 2. In the numerical section of this study, we will only consider the diffuse reflection component. This is because diffuse reflection is believed to be predominant at the altitudes of the Starshine satellites [8] and because estimating the fraction of molecules reflected in a quasi-specular fashion introduces additional uncertainty and complication to the analysis.

We will now explore the functional dependence of satellite drag on several parameters to identify the primary drivers of drag coefficients and to gain perspective on the later numerical analysis. Unless stated otherwise, the sensitivity study is performed for atmospheric temperature of 900 K, a mean molecular mass of 16 atomic mass units (atomic oxygen), $V_T = 7800$ m s^{-1}, and $T_w = 300$ K. The following equations [3] that govern FMF force coefficients on a sphere and on a flat plate facing into the flow (one side exposed to the flow) provide the baseline for exploring C_D variability:

$$C_{D,\text{sphere}} = \frac{2s^2+1}{\sqrt{\pi}s^3}\exp(-s^2) + \frac{4s^4+4s^2-1}{2s^4}\operatorname{erf}(s) + \frac{2\sqrt{\pi}}{3s}\sqrt{T_{k,r}/T_i} \tag{6a}$$

$$C_{D,\text{plate}} = \frac{2}{\sqrt{\pi}s}\exp(-s^2) + \frac{1}{s^2}(1+2s^2)\operatorname{erf}(s) + \frac{1}{s}\sqrt{\pi}\sqrt{T_{k,r}/T_i} \tag{6b}$$

where the speed ratio s is

$$s = |\mathbf{V}_T|\beta \tag{7}$$

and $\beta = \sqrt{m/(2k_bT_i)}$ while erf( ) denotes the error function defined as

$$\operatorname{erf}(x) = \frac{2}{\sqrt{\pi}}\int_0^x \exp(-t^2)\,\mathrm{d}t \tag{8}$$

Here, temperature T_i refers to the thermal temperature of the ambient gas irrespective of its bulk motion [not to be confused with the incident kinetic temperature in Eq. (4)]. Equation (5) was used to compute the reflection temperatures based on a range of accommodation coefficients expected in LEO. Figure 3 demonstrates that the drag coefficient has a strong dependence on α via its relationship with $T_{k,r}$. As mentioned previously, this parameter has been found to be a function of altitude, and the functional dependence has been explored by several researchers, most recently by Pardini et al. [18] and Pilinski et al. [24].

The drag coefficient is also sensitive to the mean molecular mass $\bar{m}$ (see Fig. 3a). To investigate how this parameter might change in the spacecraft environment, a circular orbit of varying altitude was propagated through a simulated atmosphere. The atmospheric model is the U. S. Naval Research Laboratory mass spectrometer and incoherent scatter radar extending to the exosphere, or NRLMSISE-00 [25]. In the numerical implementation, mean molecular mass is replaced by the actual mass of the two most abundant species for which the contributions are modeled separately. We limit our numerical analysis to molecular nitrogen and atomic oxygen, because these are likely to be the predominant species in the atmosphere during solar maximum at and below 400 km altitude. At solar minimum and at higher altitudes, it is important to include the contributions of helium and hydrogen. The effect of these lighter atmospheric elements is to increase C_D, as can be seen in Fig. 3a.

The total velocity magnitude V_T is seen to change the drag coefficient by only $\pm 0.9\%$ over a velocity range of ± 1000 m s^{-1}. Note, however, that the accommodation coefficient itself may be a function of V_T, so any comparative analysis should be restricted to objects flying at approximately the same speed. Furthermore, a variation of ± 100 K in the surface temperature of the spacecraft T_w results in a change in drag coefficient of approximately $\pm 1.0\%$ at full accommodation. This variability is reduced significantly at lower accommodation coefficient values. The sensitivity to atmospheric temperature is seen in Fig. 3d. A conservative atmospheric temperature error of ± 500 K results in just $\pm 0.3\%$ uncertainty in the drag coefficient of the flat plate (although the effect on slender objects with the long axis in the direction of flight is more significant [26]). It is important to remember that these sensitivities relate to the coefficient of drag C_D and not to the drag force. For example, a deviation of ± 500 K in atmospheric temperature is likely to be associated with a significant change in local atmospheric mass density, which would alter the overall drag. From these sensitivity considerations, the overall root-mean-square expected uncertainty in modeled C_D is around $\pm 2\%$. Note that, for elongated shapes, a sensitivity study is available in a report commissioned by the European Space Agency [26] as well as a paper by Sutton [27].

Given the orbit-averaged atmospheric properties, along with Eqs. (6a) and (6b), we can now investigate some representative drag coefficient values at various altitudes. Figure 4 illustrates the amount of change in drag coefficient due to changes in altitude, shape, and solar activity. The altitude and solar activity response is primarily a result of accommodation coefficient and mean molecular mass variability.

An important assumption underlying almost all the analysis techniques applicable to satellites is that the flow is in the free molecular regime characterized by a relatively high Knudsen number, $K_N > 10$. The Knudsen number, $K_N = \lambda/L$, is the ratio of a mean free path λ to a characteristic length L, and it is an indicator of the importance of intermolecular collisions relative to molecule–surface collisions. The information presented in this section is used to compute the Knudsen number using the mean free path between incident and reflected molecules. Note that this is different from the freestream Knudsen number, which is the mean free path between

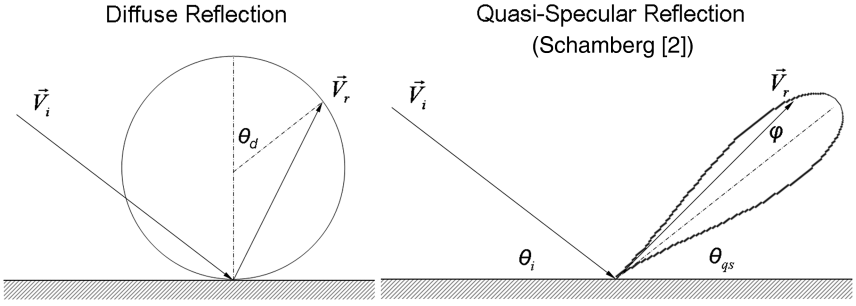

Fig. 2 The diffuse and quasi-specular reflection models.

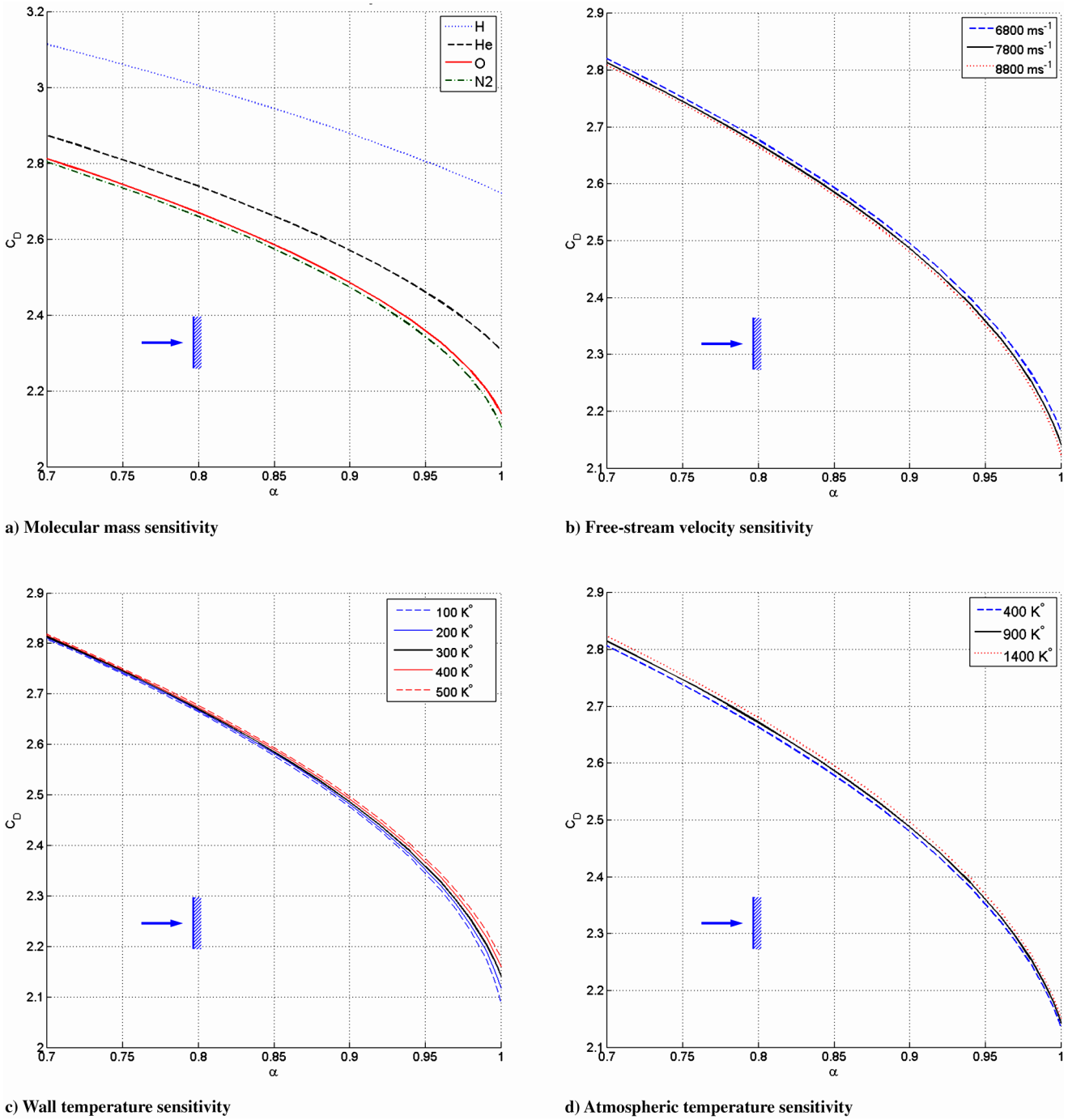

a) Molecular mass sensitivity

b) Free-stream velocity sensitivity

c) Wall temperature sensitivity

d) Atmospheric temperature sensitivity

Fig. 3 Drag coefficient sensitivity.

incident molecules only. The derivation of the incident-reflected Knudsen number for a satellite is provided by Sentman [1], and the result is shown here:

$$K_n = \frac{\sqrt{\pi}}{2n_i s\pi d^2}\sqrt{\frac{T_{k,r}}{T_i}} \tag{9}$$

where s is the speed ratio, k_B is the Boltzmann constant, n_i is the number density of the incident molecules, T_i is the temperature of the atmosphere, $T_{k,r}$ is the kinetic temperature of the reflected molecules, and d is the average of the molecular radii of the two interacting species. Applying this equation to a satellite the size of Starshine flying through the lower atmosphere at 7500 m s^{-1} leads to a Knudsen number greater than 10 above 220 km altitude at solar maximum conditions ($A_p = 5$ and $F10.7 = 225$ solar flux units). We may therefore neglect intermolecular collisions for the case of the Starshine data set. Although the data span altitudes between 200 and 470 km, the relative number of data points below 220 km amounts to less than 1% of the total data set and will not significantly change the analysis. Also, it is important to keep in mind that our formulation of the Knudsen number is quite conservative with the classical formula, predicting transition past $K_N = 10$ below 200 km altitude.

Description of Starshine Satellites and Observations

The Starshine spacecraft [6,7] were used for educational outreach and atmospheric density calibration during 1999–2003 (sunspot maximum). The primary purpose of the Starshine project is to educate school children about the effect of the atmosphere on satellite orbits. The satellites were covered by hundreds of mirrors polished by students around the world. The reflection of sunlight from these mirrors allowed the students to visually track the satellites. Starshine I was also used as the ballistic coefficient reference for

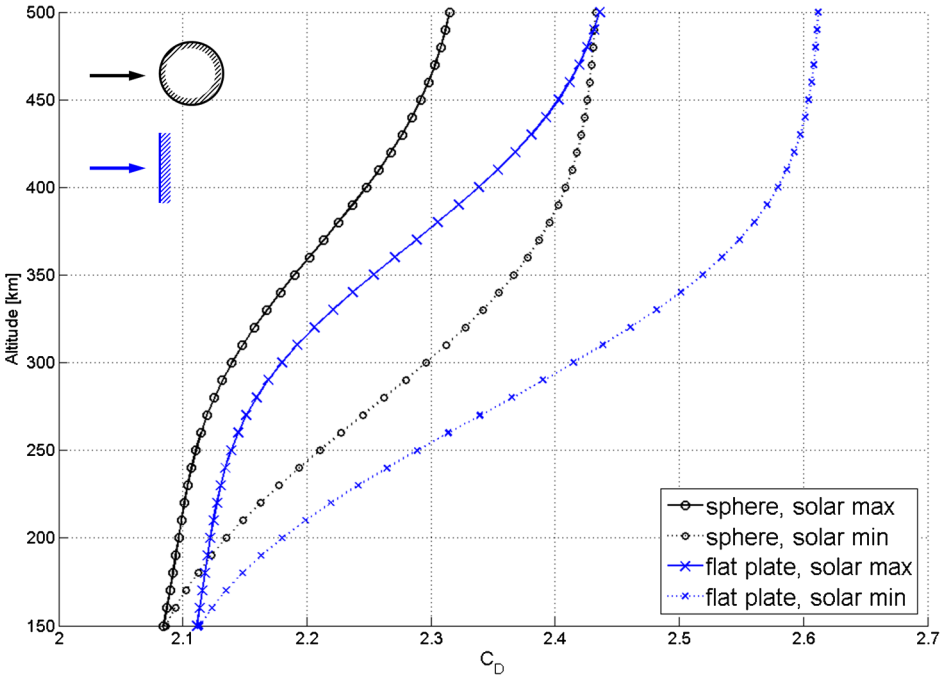

Fig. 4 The drag coefficient of a sphere and a flat plate during solar maximum and solar minimum.

global drag-derived density measurements [11–13]. These spacecraft were near spherical in the case of Starshine III and an elliptic spheroid in the case of Starshines I and II. All three spacecraft had launch vehicle adapters protruding from their surface. The most unusual features were the hundreds of 1-in.-diam mirrors that covered these satellites. The Starshines I/II and Starshine III geometries are pictured in Fig. 5. The nonspherical surface features not only altered the total surface areas but made the computation of analytical drag coefficients difficult by introducing additional uncertainties. The underlying assumption in the FMF equations used in the previous section is that a molecule interacts with any given surface only once and that the entire surface is exposed to a Maxwellian freestream velocity distribution. A concave geometry allows an incident molecule to have multiple reflections from the surface. Furthermore, the incoming velocity distribution is occluded at some points in the geometry and entirely invisible in others. A conclusion from the original analysis of the Starshine data set [8] was that the mirrors caused a 20% increase in the satellite drag coefficient of a sphere. One of the aims of this study is to model the Starshine coefficients while taking into account the concavity of the geometry to determine whether the model can be brought into agreement with the data. This will also require an adjustment to the observational data based on cross-sectional area.

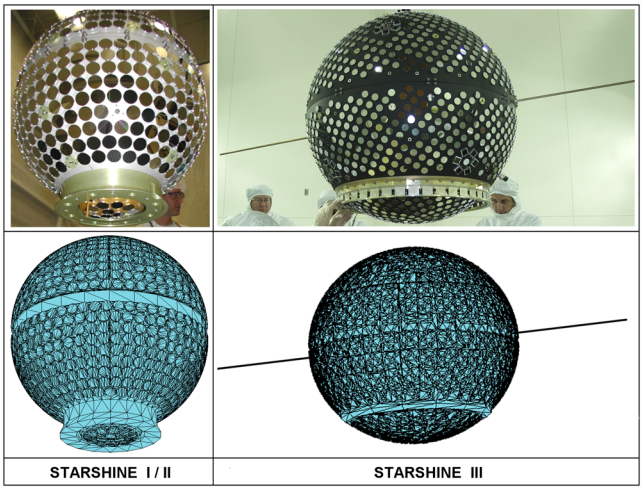

Fig. 5 Starshines I/II and Starshine III satellites along with the computational surface mesh used for each.

Table 1 shows properties of the Starshine orbits and spacecraft dimensions. Note that the cross-sectional area used to compute the drag coefficient from observed ballistic coefficients differs between our study and the previous one [10]. This is a result of recomputing the area using high-fidelity meshes of the Starshine satellites. The 2005 study [10] assumed a spherical geometry for each satellite, with the diameters adjusted slightly to account for the mirrors protruding from the surface. Since this approach explicitly omitted the exact added area of the mirrors and the launch vehicle adapters, it overestimated the measured drag coefficients. The value of this overestimate was found to be 12% for Starshines I/II and 2% for Starshine III. This is a significant difference that underlines the importance of applying the as-flown satellite dimensions to drag analysis.

Data analyzed in this study are taken from the same observations used by Bowman and Moe [10] but are scaled to adjusted cross-sectional areas producing minimum, most probable, and maximum drag coefficient values based on the extreme orientations of the geometries to the freestream as well as the statistical mode. The recomputed areas account for the entire satellite geometry, as pictured in Fig. 5. The maximum and minimum projected areas correspond to the maximum and minimum ballistic coefficient measurements and minimum and maximum observed drag coefficients, respectively. This results from the definition of the ballistic coefficient shown in Eq. (10):

$$B = \frac{C_D A}{M} \tag{10}$$

A statistical distribution of the cross-sectional areas is computed to find the most probable cross section. All three of the Starshine satellites are assumed to be tumbling in their orientation with respect to the freestream velocity. Therefore, all attitude states or angular orientations with respect to the freestream are equally probable. The cross-sectional area histograms are shown in Fig. 6 for Starshines I/II, as well as for Starshine III. The central tendency of the area used in this analysis is the mode of the distribution and indicates the most probable state. Numerical values of the areas are shown in Table 1.

Ballistic coefficient data provided by Bowman[§] include ballistic coefficients computed from the observations of satellite orbit decay

[§]B. Bowman, U. S. Air Force Space Command, Space Analysis Center, Peterson Air Force Base, Colorado, personal communication, 2008.

Table 1 Properties of the Starshine satellites

Satellite	Ref. No.	Time span	Alt. span, km	Mass, kg	A_{sphere}, m^2	$A_{min}/A_{mode}/A_{max}$, m^2	Inc., deg.
Starshine I	25,769	Jun. 99–Feb. 00	375–215	39.46	0.178	0.176/0.199/0.199	51.6
Starshine II	26,996	Dec. 01–April 02	353–216	38.56	0.178	0.176/0.199/0.199	51.6
Starshine III	26,929	Sept. 01–Jan. 03	451–221	90.04	0.685	0.697/0.699/0.706	67.0

at various altitudes and times using extensive radar tracking from a global station network [10]. Solutions to the ballistic coefficient depend on comparing drag deduced from orbits to the drag predicted by a calibrated model. We will refer to these as measured drag coefficients. Analysis of many smooth spheres has resulted in density corrections to the atmospheric model used for computing the measured drag coefficient. These density corrections are reported by Bowman and Moe [10] and reproduced here for the Jacchia 70 model in Table 2. The corrections mitigate altitude-dependent bias introduced through the use of incorrect drag coefficients in the density estimates used to construct the model. Before the area-corrected drag coefficient can be used to evaluate drag coefficient models, the measured drag coefficients are multiplied by corrections in Table 2. The resulting data set will be referred to as observed drag coefficients. Values of the observed drag coefficients are shown for the Starshine satellites in Fig. 7. The periodic signals in the data sets are a result of unmodeled density variability and have an amplitude of about ±6%. The density modeling error is removed by fitting exponential functions to each observed drag coefficient set.

Computational Method

The DSMC method models the interactions of many simulated molecules with parametrized surfaces and intermolecular collision dynamics. In this study, we employ the code DS3V (or direct simulation three-dimensional visual program) developed by Bird [3]. This program divides the flowfield into cells and selects collision partners within each cell. Recall that intermolecular collisions become important at low Knudsen numbers (below 220 km for an object the size of Starshine III), whereas all of the simulations described herein will have high Knudsen number values ($\geq$ 10), and intermolecular collisions may be neglected. The DS3V program is a convenient and configurable tool that outputs flow and surface properties, including the force coefficients in the body reference

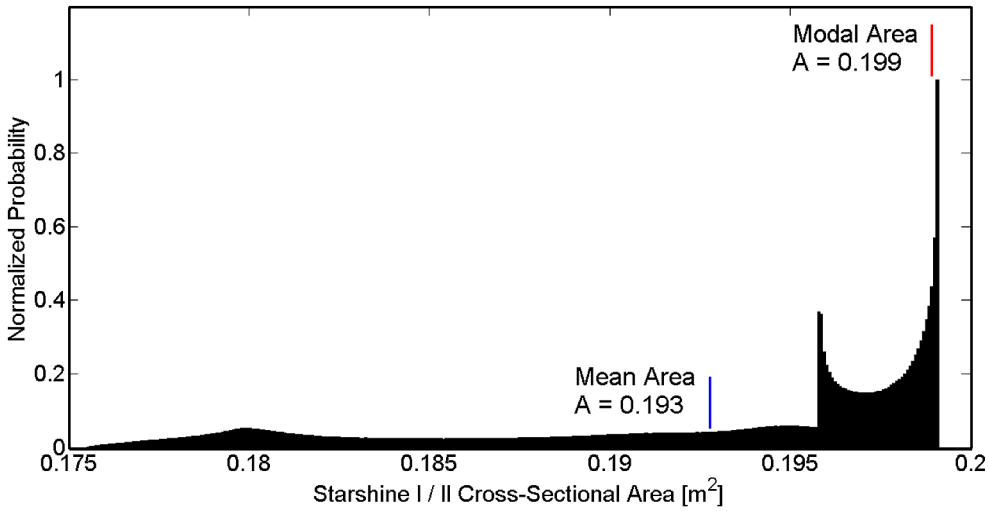

a)

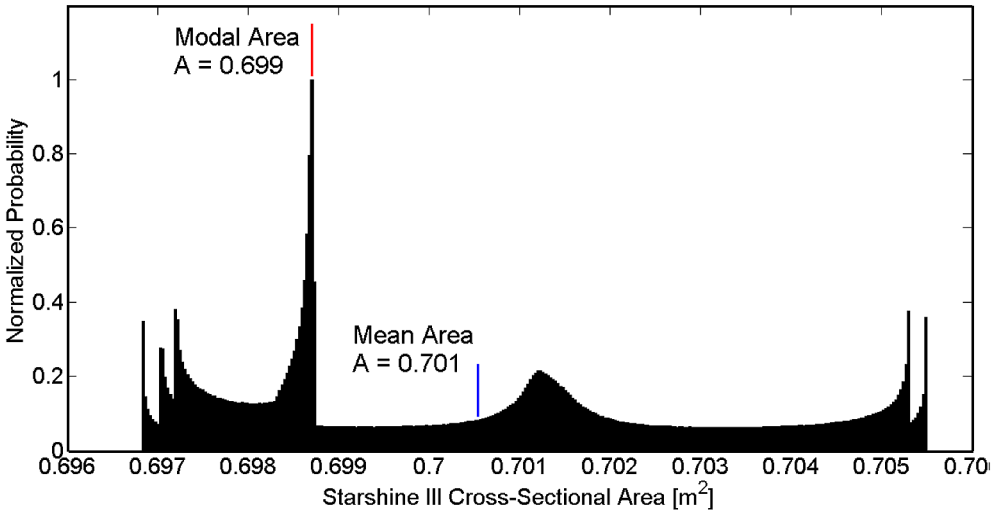

b)

Fig. 6 Cross-sectional area histograms for a) Starshines I/II and b) Starshine III geometries. Note change in scale between panels.

Table 2 Jacchia 70 density corrections as determined by Bowman and Moe [10] and used to adjust the measured drag coefficients

Altitude, km	Correction, %
200	7
250	9
300–350	11
400–500	12

frame. The simulation requires a geometry file composed of triangular elements that are imported and a surface temperature that is set to the reflection temperature $T_{k,r}$ according to the appropriate accommodation coefficient [see Eq. (5)]. It is of interest to see how the drag coefficient varies with spacecraft attitude and, to do this, the freestream velocity $-\mathbf{V}_T$ is varied according to the pitch and sideslip angles in the body coordinates, as described in Fig. 8.

The simulated force coefficients are scaled to a unit area and must be divided later by the appropriate cross-sectional area for each set of pitch and sideslip angles. We have computed the cross-sectional area as a function of the pitch angle only. This is because the Starshine satellites have sufficient symmetry around the sideslip (azimuthal) axis. Next, the aerodynamic force coefficients in the X, Y, and Z directions are projected onto the velocity vector to calculate the drag coefficient. The lift coefficients may also be easily computed but are of no interest in this particular study. Flow conditions such as the mass and ratios of molecular constituents, the atmospheric temperature, and freestream velocity are specified in an input file. This procedure is repeated for several altitudes.

The atmospheric conditions used to compute drag coefficients were retrieved using the NRLMSISE-00 atmospheric density model [25] and the horizontal wind model (HWM-07) [28]. We combined an orbital simulation with the atmospheric model in order to closely represent orbital conditions. Three- to five-day periods along the observation time scales were chosen for the simulations, and the spacecraft altitude and geographic location were entered into the atmospheric models along with historical indices of solar activity. Solar activity indicators used in this study are $F10.7$ solar and A_p geomagnetic measurements, and they are inputs into the NRLMSISE-00 model. The $F10.7$ index is a ground-based measurement of the solar flux at the 10.7 cm wavelength. Meanwhile, the planetary A_p index is a scaled value of geomagnetic activity based on magnetic field variability observed by a system of globally distributed magnetometers. Both A_p and $F10.7$ attempt to quantify the relative effect of solar activity on the thermosphere and can be used to adjust atmospheric models accordingly. The indices are shown in Fig. 9 along with the orbit lifetimes of the three Starshine satellites, as well as several other observation objects. Average atmospheric composition, temperature, and freestream velocity resulting from the orbital simulations were saved for the numerical computation of drag coefficients. Figure 9 indicates that Starshine satellites flew at varying levels of solar activity. To account for these variations, accommodation coefficients were computed using a model developed by Pilinski et al., which describes the accommodation coefficient as a function of atomic oxygen partial pressure [24]. The partial pressure was estimated using NRLMSISE-00 outputs at the satellite position.

The DS3V code is relatively fast and efficient, allowing for the computation of forces on any arbitrary surface mesh [29]. At the time of writing, there were two disadvantages to the DS3V program when it came to computing satellite drag coefficients. First, only specular and diffuse reflections were treated. When using the DS3V code, we limited ourselves to the diffuse model because of the unrealistic nature of specular reflection on engineering materials and because of the relative success of diffuse reflection in describing the drag coefficient of contaminated surfaces [21]. The second disadvantage was that DS3V did not allow accommodation other than $\alpha = 1$ in the diffuse model. To get around this problem, the surface temperature was set to the appropriate reflection temperature. The result was that each molecule was reflected at the same energy, even though it may have interacted with the surface multiple times and thus accommodated more fully to the surface temperature. We have included a second model in our analysis to compute a correction to DS3V resulting from greater accommodation caused by multiple reflections. This code was a test particle Monte Carlo method [5] implemented in MATLAB® and applied to an arbitrary surface mesh. The advantage of this program was that it allowed for both fixed-temperature reflections (single-impact accommodation) as well as recurring accommodation reflections (multi-impact accommodation), wherein the reflection temperature was computed each time based on the incoming velocity of the reflected molecules and the accommodation coefficient ascribed to the surface. The modification of DS3V to include additional reflection models and incomplete accommodation in diffuse reflections is left as a subject of future work. Note that results from single-temperature (single-impact accommodation) reflections and recurring accommodation (multi-impact accommodation) reflections serve as two extremes of behavior for multiply reflected molecules. Single-impact accommodation assumes that no energy is lost after the first reflection when the molecule accommodates to a reflection temperature $T_{k,r}$.

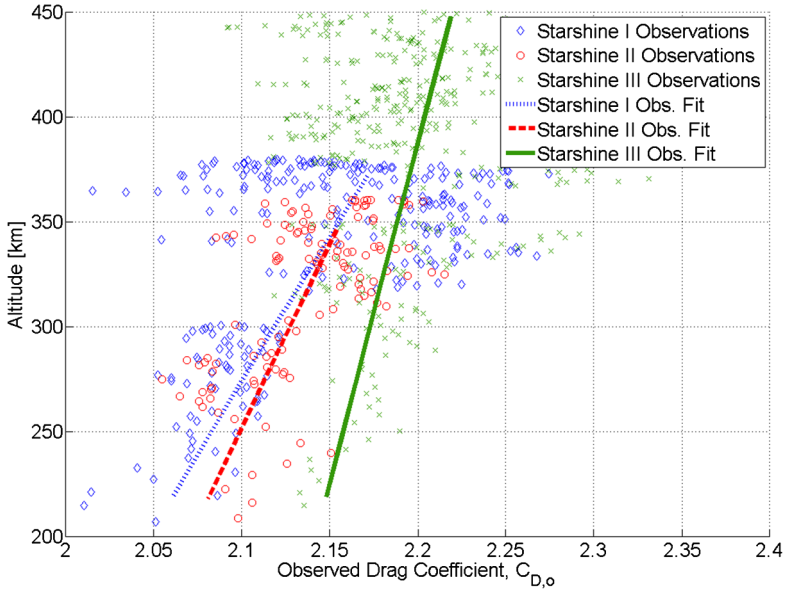

Fig. 7 Observed drag coefficients plotted along altitude and observation fits for the three Starshine satellites.

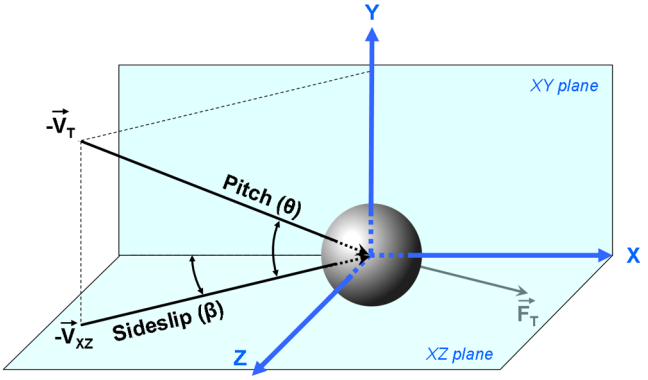

Fig. 8 Simulation geometry.

Multi-impact accommodation holds that, for any one molecule, each successive reflection on the surface is accompanied by successive accommodations and that the molecule reflection temperatures approach closer to T_w with every gas–surface interaction. It is quite possible that the reality for most gas–surface interactions lies between the two extremes. Laboratory experiments indicate that accommodation may be a function of incident kinetic energy [30,31]. The experiments performed by Doughty and Schaetzle [31], as well as the paddle-wheel measurements of Explorer 6 [32], dealt with contaminated surfaces and energy ranges at and above the theoretical binding energy of the contaminants. The results from these references indicate that, at higher incident velocities, the energy loss is diminished. Meanwhile, the experiment performed by Winters et al. [30] included data from uncontaminated surfaces at energies corresponding to molecules reflected from satellite surfaces. These data suggest that energy loss may also become less complete at lower values of kinetic energy. One possible explanation for the two sets of results is that there may exist an optimal range of energies for energy accommodation. Molecules that approach the surface with kinetic energies below this range, such as those reflected from another region of the satellite, undergo less energy loss than the molecules approaching in the optimal range. Similarly, molecules that approach the surface above the optimal kinetic energy range, such as those that exist in the conditions of high-velocity perigee passes, also reflect from the surface with less energy loss than molecules approaching with energies corresponding to LEO speeds.

In addition to numerical solutions, observed drag coefficients are also compared with two analytical methods. The first analytical model will be the equation for drag on a sphere [Eq. (6a)] and is the method employed in all previous Starshine analyses. The second model computes the drag coefficient of each surface element [Eq. (6b)] in the Starshine mesh and combines it to form the drag coefficient of the entire object. The analytical solutions are carried out for N species considered in the computation and combined as a weighted mean using Eq. (11):

$$C_{D,\text{composite}} = \frac{\sum_{j=1}^{N} C_{D,j} n_j m_j}{\sum_{j=1}^{N} n_j m_j} \tag{11}$$

These analytic approaches do not treat secondary reflections or shadowing inside concave geometries such as the Starshine satellite surfaces. They are used as points of reference for quantifying the improvement in drag coefficients afforded by the numerical techniques.

Model Results

The effect of surface features on the drag coefficient was examined via DS3V computation at full accommodation and a variety of pitch angles for Starshines I/II geometry. Figure 10 shows the differences in drag coefficient resulting from the oblate shape of the satellite, the adapter ring, and the hundreds of mirrors covering the surface. These results were generated using an accommodation coefficient of 1.00, a freestream velocity of 7800 m s^{-1}, an atmospheric temperature of 1100 K, and a surface temperature of 300 K. As the shape deviates from spherical, the drag coefficient is lowered for most pitch angles θ ($\theta = \pm 90°$ points along the axis of symmetry, looking either at $(-)$ or away from $(+)$ the adapter ring, with $\theta = 0°$ corresponding to the freestream oriented in the equator of the geometry). Furthermore, while the oblateness and the addition of the adapter ring raise the drag coefficient with respect to that of a sphere at certain values of θ and lower it at other values, the myriad of mirrors located on the hemispheres raise the average C_D and increases its variability. To discover the reason for this C_D increase, a flat plate covered with circular extrusions like the Starshine mirrors was modeled at 45° to the freestream using the test particle code. Reflected molecules were binned according to angle of reflection, and the resulting distribution is shown in Fig. 11. The distribution exhibits an enhancement at 45° to the surface normal (back toward the freestream direction) and a component near 90°. Both directions are indicated by solid arrows in Fig. 11. These two components facing back into the freestream serve to increase the momentum change in that direction and increase the drag coefficient.

Next, we examine the drag coefficient of Starshine III as a function of angle of attack. This study was performed at several values of accommodation. The drag coefficient profile is similar to that of Starshines I/II but exhibits more symmetry with respect to positive and negative values of θ. This result is consistent with the fact that Starshine III geometry resembles a sphere more closely than the geometries of Starshine I and II. As the analytical study in the section on the physics of drag coefficients would already suggest, the drag coefficients of the Starshine satellites also increase with lower values of accommodation.

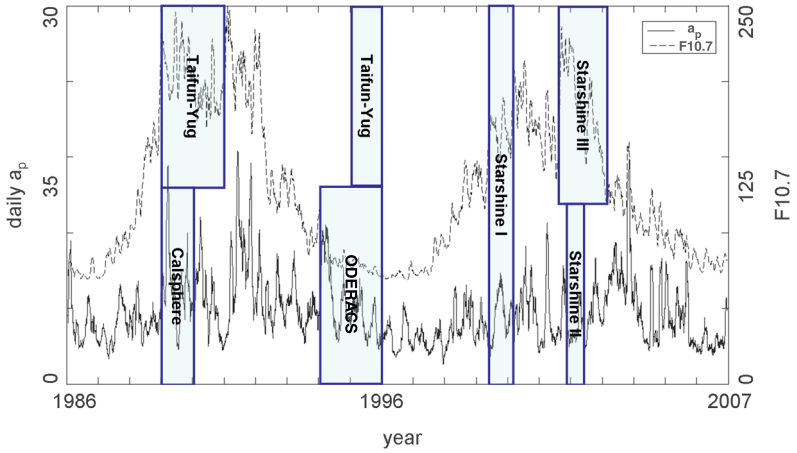

Fig. 9 Starshine and ODERACS orbit life spans overlaid on solar activity histories. Taifun-Yug and Calsphere satellites are additional tracking objects used by Pilinski et al. [24] to constrain the accommodation coefficient.

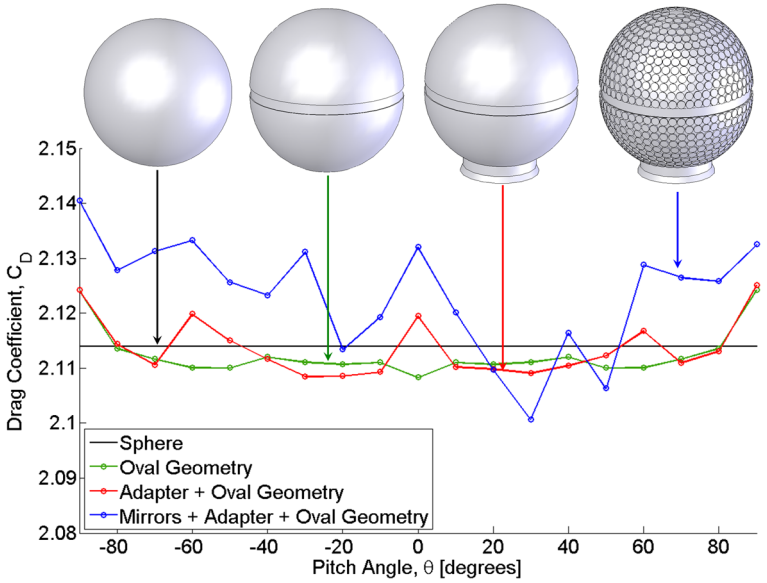

Fig. 10 DSMC values of Starshines I/II drag coefficients as a function of pitch angle at full accommodation ($\alpha = 1.00$).

To take into account the compounding effect of multiple reflection on energy loss, the temperature of reflection must be varied along successive surface collisions of each molecule. Several test particle runs were carried out for full Starshines I/II and Starshine III geometries to compute the difference between a Starshine with mirrors (rough) and a Starshine without mirrors (smooth). The resulting corrections are shown in Fig. 12 and can be applied to the fixed reflection temperature (DS3V) data. Figure 12 illustrates the effect of adding mirrors on C_D for Starshines I/II and Starshine III under the case of both multi-impact accommodation (variable $T_{k,r}$) and single-impact accommodation (fixed $T_{k,r}$). It is of interest to derive some analytical expressions for multiple-impact accommodation of molecules to closer examine changes in effective accommodation. The theoretical approximations will also help estimate corrections to a drag coefficient computed using a fixed $T_{k,r}$. Equation (12) describes the temperature of reflection $T_{k,r,n}$ experienced by a molecule that interacts with the surface for the nth time. This expression was obtained by recursive substitution of Eq. (5):

$$T_{k,r,n} = (1-\alpha_0)^{n+1} \cdot T_{k,i,0} + (1-\alpha_0)^n \cdot \alpha_0 \cdot T_w + \cdots + (1-\alpha_0)^0 \cdot \alpha_0 \cdot T_w \tag{12}$$

If we substitute Eq. (12) into the definition of accommodation coefficient [Eq. (3)] and consider the resulting multiple-reflection coefficient, or effective accommodation, as a function of number of secondary reflections n, we see that even a small number of reflections could drastically change the energy loss of molecules. For example, starting at a coefficient of 0.85, two reflections are sufficient to bring the effective coefficient to 1.00. To find the effect that this has on C_D, the fraction of molecules undergoing secondary reflections is now quantified. Equation (13) expresses this as an empirically determined fraction f_n of molecules to have undergone at least n reflections:

$$f_n = \begin{cases} (1-a) & \text{if } n = 0, \text{ primary reflection} \\ ae^{-b(n-1)} & \text{if } n \geq 1, \text{ at least } n \text{ reflections} \end{cases} \tag{13}$$

This equation can be thought of as a leak rate or diffusion from a cavity, where a is the fraction of molecules to continue undergoing collisions after the original reflection and b is the rate at which molecules leave the cavity thereafter. Both a and b can be determined via Monte Carlo analysis of a specific geometry. In the case of satellites with surface irregularities, the diffusion takes place in an array of cavities, but the same expression still holds. Next, the number of molecules that leave the surface after exactly n reflections is written as $FC_n = f_n - f_{n+1}$, resulting in Eq. (14). The values of a and b along with the diffusion curves for the two Starshine geometries were estimated using the test particle Monte Carlo program, and they are presented in Fig. 13. Note that the higher density of mirror coverage (68 versus 30%) on Starshines I/II causes

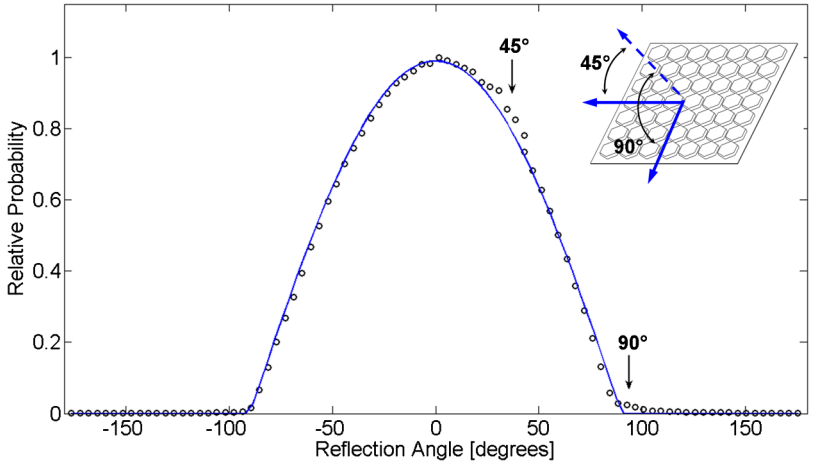

Fig. 11 A reflection distribution from a plate segment covered in circular extrusions subject to incoming molecules at 45°.

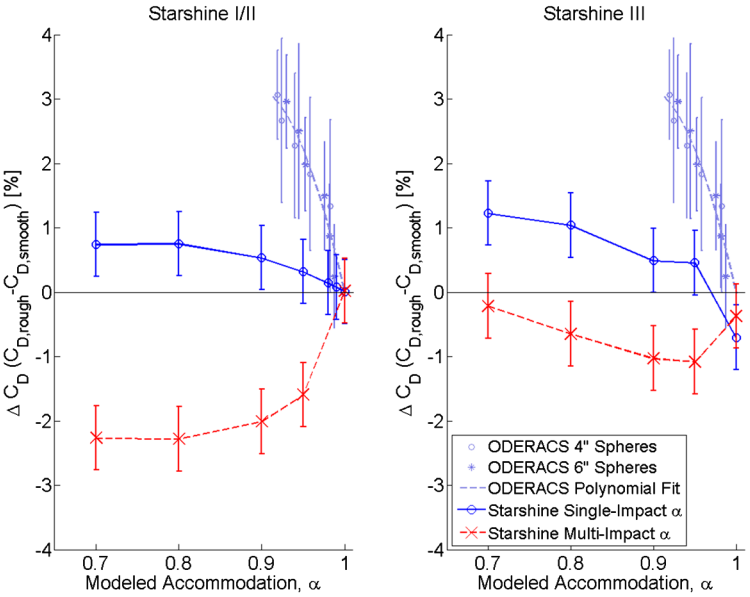

Fig. 12 Modeled corrections to the drag coefficient caused by concave geometry for single-impact and multi-impact accommodation cases. ODERACS experiment data are shown for reference.

the average molecule to leave the surface after having undergone more reflections:

$$FC_n = \begin{cases} (1-a) & \text{if } n = 0 \\ a(e^{-b(n-1)} - e^{-bn}) & \text{if } n \geq 1 \end{cases} \tag{14}$$

Finally, Eq. (15) combines the drag coefficients of each group of molecules for the appropriate accommodation. The formulas described previously have been found to reproduce the simulated 3–4% correction within 25% accuracy for the multi-impact accommodation case. Therefore, they may be used for an order-of-magnitude estimate of drag coefficient reduction due to multiple accommodations before investing significant computation time for the numerical simulation. Note that these approximations predict a maximum efficiency of drag reduction due to multiple-impact accommodations at an accommodation of approximately 0.7–0.8 and that the location of this peak efficiency is almost invariant to the flow conditions:

$$C_{D,\text{effective}} = \sum_{n=1}^{\infty} C_D(T_{k,r,n}) \cdot F_n \tag{15}$$

Figure 14 shows the Starshine observed drag coefficients plotted together with the Monte Carlo modeled coefficients at various values of altitude. Three sources of data and their exponential fits are shown on the plot. The data correspond to computation of the observed drag coefficient using modal and average areas, as well as the previously used adjusted spherical area. Both multi-impact (variable $T_{k,r}$) and single-impact (fixed $T_{k,r}$) models are shown for the satellites. The relative reduction of the drag coefficient by multiple reflections brings the multi-impact accommodation model and modal-area data into closer agreement, especially at altitudes below 350 km. The same is true of the average-area data and the single-impact accommodation model. Although the modal area is taken as the correct value, the difference between the modal-area fit and the mean-area fit (3% for Starshines I/II and 0% for Starshine III) can serve as an uncertainty estimate in the observed drag coefficient fit due to cross-section accuracy. All model comparisons with the data indicate that there is room for improvement above 350 km altitude. This may be due to a small fraction of quasi-specular reflection, which is not included in the present study. It could also be a result of the accommodation coefficient model used to model drag coefficients.

Analytical results are shown in Fig. 14. These results are within 5% of either numerical model at all altitudes, meaning that a plate model or geometric approximation serves as a good first-order estimate of even complex drag coefficients. Table 3 lists the numerical and analytical modeling results for the three Starshine satellites at a number of different altitudes. Since both numerical models straddle the observations, it is difficult to conclude which model of reflections is more accurate based on Starshine data alone. The multi-impact accommodation model lowers the drag coefficient of Starshine with respect to a sphere and agrees closer with the modal-area estimate, which is taken to be the better observed value.

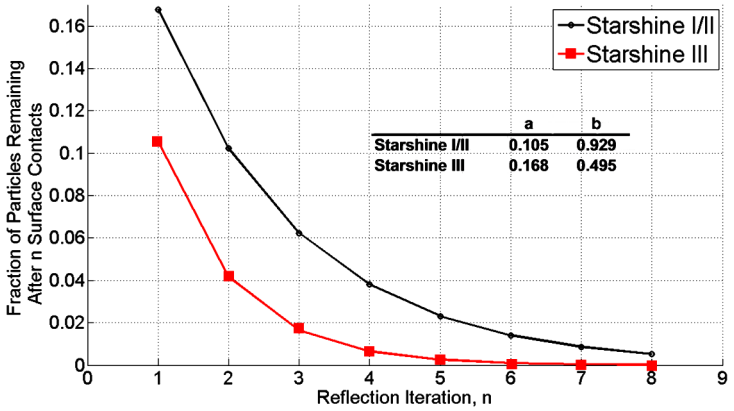

Fig. 13 The relative amount of molecules undergoing at least *n* multiple reflections.

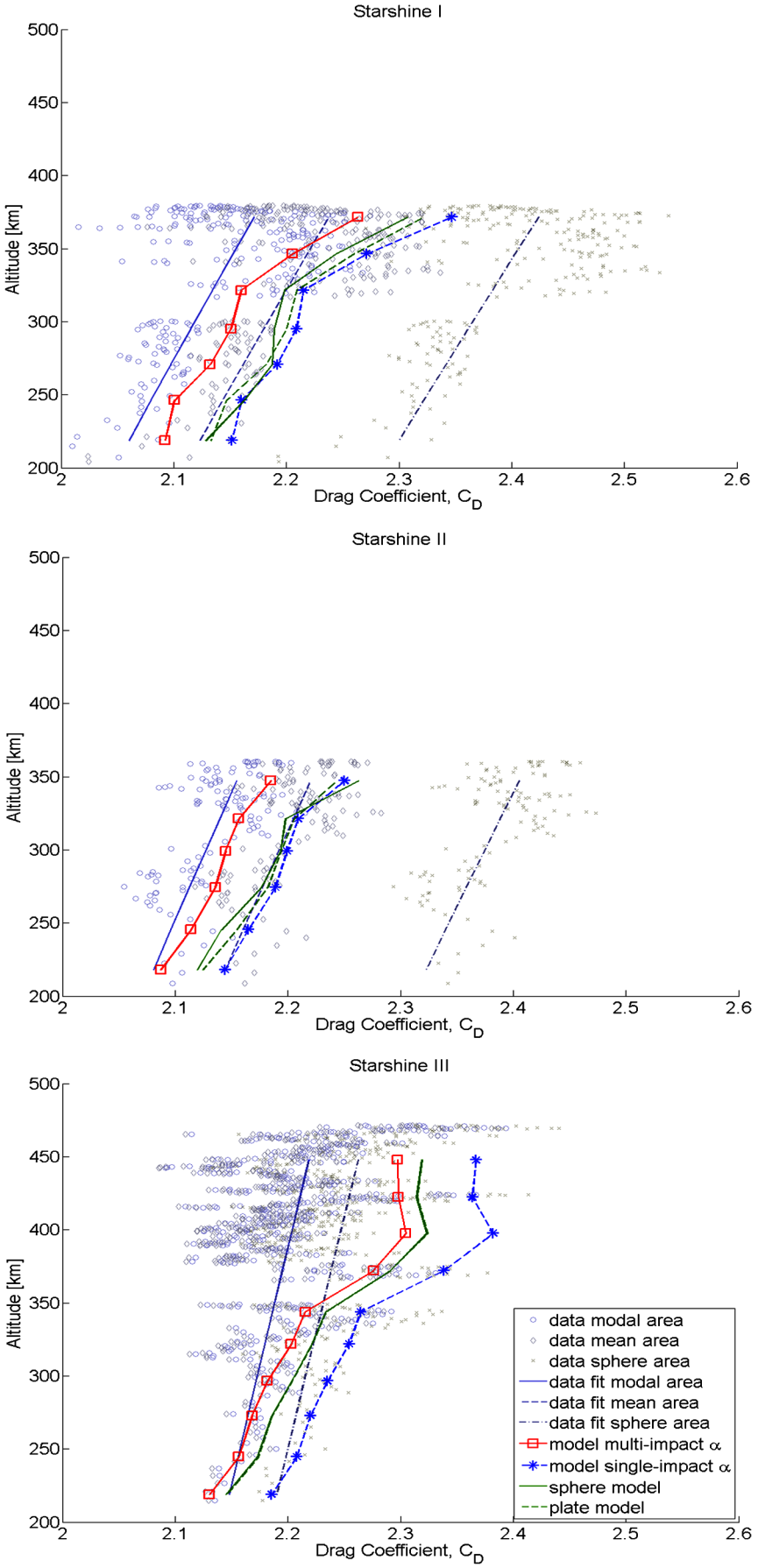

Fig. 14 Starshine I, II, and III modeled drag coefficients along with Monte Carlo values for multiple-impact and single-impact accommodation.

Table 3 Drag coefficient model inputs and results

Sat.	Altitude, km	T_{atm}, K	n_O, m^{-3}	n_{N2}, m^{-3}	α	$C_{D,sphere}$	$C_{D,FMF}$	$C_{D,nmrcal}$. $T_{k,r}$ fixed	$C_{D,nmrcal}$. $T_{k,r}$ variable
I	371.6	1037	1.91×10^{14}	2.15×10^{13}	0.924	2.321	2.322	2.347	2.263
	346.5	1095	4.57×10^{14}	5.86×10^{13}	0.953	2.256	2.260	2.271	2.206
	321.6	1079	6.09×10^{14}	1.10×10^{14}	0.974	2.205	2.209	2.215	2.160
	294.9	1019	7.68×10^{14}	1.90×10^{14}	0.976	2.196	2.200	2.208	2.151
	270.8	1025	1.21×10^{15}	3.91×10^{14}	0.982	2.178	2.182	2.192	2.132
	246.4	1055	2.02×10^{15}	9.03×10^{14}	0.991	2.143	2.147	2.160	2.105
	218.7	1029	3.56×10^{15}	2.28×10^{15}	0.994	2.129	2.133	2.152	2.093
II	347.3	1209	5.40×10^{14}	9.61×10^{13}	0.961	2.240	2.244	2.250	2.185
	321.3	1159	7.63×10^{14}	1.46×10^{14}	0.976	2.201	2.206	2.209	2.157
	299.2	1105	1.02×10^{15}	2.17×10^{14}	0.979	2.190	2.194	2.199	2.145
	274.2	1106	1.58×10^{15}	4.59×10^{14}	0.983	2.178	2.182	2.189	2.136
	245.6	1125	2.58×10^{15}	1.07×10^{15}	0.990	2.151	2.155	2.165	2.114
	218.1	1097	4.34×10^{15}	2.76×10^{15}	0.996	2.121	2.125	2.144	2.087
III	447.8	1265	1.48×10^{14}	1.40×10^{13}	0.923	2.319	2.319	2.367	2.298
	422.3	1174	1.70×10^{14}	1.22×10^{13}	0.925	2.314	2.315	2.364	2.298
	397.6	1040	1.19×10^{14}	1.15×10^{13}	0.916	2.323	2.324	2.382	2.305
	372.1	1082	2.75×10^{14}	2.77×10^{13}	0.936	2.291	2.291	2.338	2.276
	343.9	1147	4.78×10^{14}	7.91×10^{13}	0.964	2.233	2.234	2.264	2.215
	321.8	1072	5.41×10^{14}	1.12×10^{14}	0.968	2.221	2.222	2.254	2.203
	296.6	1089	7.48×10^{14}	2.24×10^{14}	0.974	2.204	2.204	2.235	2.182
	272.8	986	9.57×10^{14}	3.27×10^{14}	0.979	2.186	2.186	2.220	2.168
	244.7	1016	1.70×10^{15}	8.12×10^{14}	0.983	2.173	2.174	2.208	2.156
	219.0	934	2.63×10^{15}	1.62×10^{15}	0.990	2.145	2.146	2.185	2.131

On the other hand, the angular distribution of molecules reflected from an irregular or rough sphere should increase the drag coefficient, as shown in Fig. 10, and this more intuitive model agrees well with average-area observations. To address this question, we turn to an experiment called ODERACS (orbital debris radar calibration spheres) [10]. The ODERACS tracking objects included sandblasted and smooth metallic spheres flying in the same orbit. For both the 4 and 6 in. ODERACS spheres, the sandblasted spheres exhibited up to 3% greater drag coefficients. To make a better comparison of ODERACS data and our numerical models, the data were plotted as a function of accommodation based on a semi-empirical model described in a previous paper [24]. The results for both 4 and 6 in. ODERACS spheres are shown in both panels of Fig. 12 for comparison with the Starshine drag coefficient models. The data on the plots are 30 point averages of the observed difference between the rough and smooth sphere measured drag coefficients. The uncertainty is shown in the figure as the standard deviation of each 30 point set. When plotted as a function of modeled accommodation, both the 4 and 6 in. data points overlap on a single curve, which goes to zero as accommodation goes to unity. The variation of accommodation along the ODERACS data sets is primarily the result of a continuous change in mean altitude. This indicates that the difference between a rough and smooth surface diminishes as the accommodation reaches a value of one, with the rough surface having a greater drag coefficient at lower values. The increase in drag coefficient can be explained by surface irregularities that protrude from the sphere and, at the object edge, preferentially reflect molecules into the flow direction, as explained by Moe and Bowman [8]. Like a flat plate, the protrusions have a C_D curve that grows faster with a decrease in accommodation than the C_D of a sphere. This is the same phenomenon that is partially responsible for the drag coefficient curves for a flat plate and sphere in Fig. 4 to converge at higher values of accommodation (lower altitudes). Figure 12 indicates that the single-impact accommodation model for Starshines I/II and III agrees qualitatively with ODERACS observations. The quantitative difference between ODERACS and the Starshine models is most likely due to differences in surface geometry and degree of surface roughness. For both Starshine geometries, the addition of the mirrors in the single-impact model increases the drag coefficient by approximately the same amount (1%). The model comparison with the ODERACS spheres indicates that a single-impact accommodation case may be more appropriate for use with Earth-orbiting satellites. This implies that reflected molecules accommodate far less than those arriving to the surface from the freestream. Possible reasons for this include recombination on the surface and energy dependence of the accommodation coefficient.

The results from the previous analysis combined with previous accommodation coefficient measurements in a highly eccentric orbit suggest that there could be an optimum incident kinetic energy $E_{k,i}$ where satellite accommodation coefficients are highest. The first piece of supporting evidence is that reflected molecules with energies near 0 eV accommodate much less than the molecules colliding directly from the freestream. If this was not the case, the drag coefficient of a rough sphere would actually be lower, as indicated in Fig. 12. The reduction in accommodation is consistent with laboratory findings by Winters et al. [30], which show that for noble gases, there is a drop in the fraction of kinetic energy deposited at the surface as the incident energy is reduced to 0 eV. It is important to note that Winters et al. measured fraction of kinetic energy deposited on the surface as opposed to the accommodation coefficient, and that this laboratory experiment did not account for adsorption. While the laboratory data collected by Winters et al. indicated a plateau in the high-energy response of kinetic energy deposited on the surface, previous accommodation measurements from a highly eccentric orbit of Explorer 6 [17,32] (with freestream energies at perigee greater than 5 eV) found lower accommodation values than those measured in (5 eV atomic oxygen) orbit. The decrease in α at higher energies may be a result of lower levels of surface contamination caused by a decrease in adsorption efficiency at incident energies in highly eccentric orbits. Accordingly, accommodation appears to be more complete in the vicinity of 5 eV (incoming atomic oxygen for circular or low-eccentricity orbits) than it is at either 0–1 eV (reflected molecules) or for energies much greater than 5 eV (highly eccentric orbits). To attain a better understanding of accommodation as a function of kinetic energy of the incoming molecules, more data will need to be analyzed from highly eccentric orbits.

Following the drag coefficient analysis, the ballistic coefficient of Starshine I, which was used as a reference for drag-derived density data, can now be corrected. The ballistic coefficient values used in past density studies were 0.009248 m^2 kg^{-1} ($C_D = 2.1$) [11,12] and 0.009744 m^2 kg^{-1} ($C_D = 2.2$) [13]. Using modal and mean cross-sectional area distributions along with drag coefficients computed in this paper results in values of 0.0105–0.0118 m^2 kg^{-1}, depending on altitude. This amounts to a 8–25% altitude-dependent correction in the densities derived in the previous studies.

Conclusions

Drag coefficients of the Starshine satellites were simulated using both numerical (Monte Carlo) approaches and analytical models. Freestream conditions used in these simulations were obtained from atmospheric modeling along the satellite orbits. The Starshine spacecraft were covered with hundreds of mirrors that protruded from the surface and created trenchlike concavities between the mirrors. Our study revealed that taking into account secondary reflections inside the cavities increases the drag coefficient slightly (approximately 1%) of a spherical or near-spherical object with surface irregularities. The modeled drag coefficients agree with the observed drag coefficients to within 3–5%, an improvement over the 20% discrepancy observed in previous studies. Taking into account the spherically-based area estimates results in 3–4% of this improvement. The agreement was especially good below 350 km, where atomic oxygen adsorption dominates, and the reflection is most likely entirely diffuse. All models deviated from observations above 350 km. The ballistic coefficient was found to be 0.0105–0.0118 $m^2\ kg^{-1}$ for Starshines I/II and 0.0169–0.0185 $m^2\ kg^{-1}$ for Starshine III. Therefore, drag-derived density data sets that used Starshine I as a reference with a ballistic coefficient of 0.00925–0.009744 $m^2\ kg^{-1}$ should be reduced by 8–25%.

The increase in drag coefficient accuracy afforded by the use of Monte Carlo models and accommodation coefficients extrapolated to levels of solar activity translates directly into improvements in derivation of density from drag. These models also better our ability to predict satellite orbits. As has been shown throughout this paper, gas–surface interactions and, especially, energy accommodation values are the core drivers of drag coefficient determination for any particular geometry. Lack of detailed knowledge of the gas–surface interaction is the greatest limiting factor for the application of numerical models. Progress must be made in this area in order to further reduce the errors in atmospheric drag estimation.

Our results show that concave features can increase the drag of satellites covered with surface irregularities when the accommodation of reflected molecules is much less complete than that of incident molecules (single-impact accommodation model). Such a model leads to an increase in drag coefficient of a rough object, which is enhanced at lower values of accommodation. The increase is caused by portions of the flow being reflected back toward the freestream direction. This result is in qualitative agreement with data from the ODERACS spheres [10], which also indicate a difference between rough and smooth surface drag coefficients that grows with a decrease in accommodation.

The modeling of the Starshine drag coefficients improved both the absolute and relative agreement between the model and the data. The remaining discrepancies may be due to differences in surface composition between the different satellites as well as uncertainty in the accommodation coefficients. The large uncertainty in the cross-sectional areas of Starshines I/II may also be a factor in the remaining errors. Another source of error may be the atmospheric model used to derive measured drag coefficients. Because of the inherent uncertainties of estimating drag coefficients in orbit and the small differences between analytical and numerical techniques, it is difficult to validate an improvement in modeling for the numerical techniques. One clear advantage of numerical modeling is interchangeability of the gas–surface interaction model with any arbitrary shape. This is demonstrated by the ability of numerical models to reproduce the differences between rough and smooth objects.

Acknowledgments

This work was supported by the Neutral Atmosphere Density Interdisciplinary Research Program Multidisciplinary University Research Initiative, under grant FA9550-07-1-0565, sponsored by the U. S. Air Force Office of Scientific Research to the University of Colorado at Boulder. Scott Palo was supported by the National Science Foundation grant ATM-0449985. The authors would like to thank Bruce Bowman for the fitted ballistic coefficient data, Gilbert Moore for providing detailed information regarding the Starshine satellite dimensions, and Kenneth and Mildred Moe and Eelco Doornbos for their helpful advice with the paper.

References

[1] Sentman, L. H., "Free Molecule Flow Theory and its Application to the Determination of Aerodynamic Forces," Lockheed Missiles and Space Co. TR LMSC-448514, 1961.

[2] Schamberg, R., "Analytic Representation of Surface Interaction For Free Molecule Flow with Application to Drag of Various Bodies," *Aerodynamics of the Upper Atmosphere*, RAND Corp. Rept. R-339, Santa Monica, CA, 1959, pp. 12-1–12-41.

[3] Bird, G. A., *Molecular Gas Dynamics and the Direct Simulation of Gas Flows*, Oxford Science, New York, 1994.

[4] Bird, G. A., "Recent Advances and Current Challenges for DSMC," *Computers and Mathematics with Applications*, Vol. 35, No. 1, 1998, pp. 1–14.
doi:10.1016/S0898-1221(97)00254-X

[5] Davis, D. H., "Monte Carlo Calculation of Molecular Flow Rates Through a Cylindrical Elbow and Pipes of Other Shapes," *Journal of Applied Physics*, Vol. 31, No. 7, 1960, pp. 1169–1176.
doi:10.1063/1.1735797

[6] Braun, B., Butkiewicz, C., Sokolsky, I., and Vasquez, J., "The Starshine Satellite: From Concept to Delivery in Four Months," 13th Annual AIAA/USU Conference on Small Satellites, Utah State Univ. Paper SSC99-I-7, North Logan, UT, 1999.

[7] Jenkins, P., "Results from the Advance Power Technology Experiment on the Starshine 3 Satellite," 16th Annual AIAA/USU Conference on Small Satellites, Utah State Univ. Paper SSC02-X-3, North Logan, UT, 2002.

[8] Moe, K., and Bowman, B. R., "The Effects of Surface Composition and Treatment on Drag Coefficients of Spherical Satellites," AAS/AIAA Astrodynamics Specialist Conference, American Astronautical Soc. Paper 05-258 Springfield, VA, 2005.

[9] Bowman, B. R., and Storz, M. F., "High Accuracy Satellite Drag Model (HASDM) Review," American Astronautical Soc., Paper 03-625, 2003.

[10] Bowman, B. R., and Moe, K., "Drag Coefficient Variability at 175–500 km from the Orbit Decay Analyses of Spheres," AAS/AIAA Astrodynamics Specialist Conference, American Astronautical Soc. Paper 05-257, 2005.

[11] Lean, J. L., Picone, J. M., Emmert, J. T., and Moore, G., "Thermospheric Densities Derived from Spacecraft Orbits: Application to the Starshine Satellites," *Journal of Geophysical Research*, Vol. 111, 2006, Paper A04301.
doi:10.1029/2005JA011399

[12] Emmert, J. T., Meier, R. R., Lean, J. L., and Christensen, A. B., "Thermospheric Density 2002–2004: TIMED/GUVI Dayside Limb Observations and Satellite Drag," *Journal of Geophysical Research*, Vol. 111, No. A10, 2006, Paper A10S16.
doi:10.1029/2005JA011495

[13] Emmert, J. T., "A Long-Term Data set of Globally Averaged Thermospheric Total Mass Density," *Journal of Geophysical Research*, Vol. 114, 2009, Paper A06315.
doi:10.1029/2009JA014102

[14] Moe, K., Moe, M. M., and Wallace, S. D., "Improved Satellite Drag Coefficient Calculations From Orbital Measurements of Energy Accommodation," *Journal of Spacecraft and Rockets*, Vol. 35, No. 3, 1998, pp. 266–272.
doi:10.2514/2.3350

[15] Cook, G. E., "Satellite Drag Coefficients," *Planetary and Space Science*, Vol. 13, No. 10, 1965, pp. 929–946.
doi:10.1016/0032-0633(65)90150-9

[16] Moe, M. M., and Wallace, S. D., "Refinements in Determining Satellite Drag Coefficients: Method for Resolving Density Discrepancies," *Journal of Guidance, Control, and Dynamics*, Vol. 16, No. 3, 1993, pp. 441–445.
doi:10.2514/3.21029

[17] Moe, K., and Moe, M., "Gas–Surface Interactions and Satellite Drag Coefficients," *Planetary and Space Science*, Vol. 53, No. 8, 2005, pp. 793–801.
doi:10.1016/j.pss.2005.03.005

[18] Pardini, C., Anselmo, L., Moe, K., and Moe, M., "Drag and Energy Accommodation Coefficients During Sunspot Maximum," *Advances in Space Research*, Vol. 45, No. 5, 2010, pp. 638–650.
doi:10.1016/j.asr.2009.08.034

[19] Schaaf, S. A., and Chambre, P. L., *Flow of Rarefied Gases*, Princeton Univ. Press, Princeton, NJ, 1961.

[20] Gregory, J. C., and Peters, P. N., "A Measurement of the Angular Distribution of 5 eV Atomic Oxygen Scattered off a Solid Surface in Earth Orbit," *Proceedings of the 15th International Symposium on Rarefied Gas Dynamics*, Stuttgart, Germany, Vol. 2, edited by B. G. Teubner, Academic Press, New York, 1987, pp. 644–654.

[21] Moe, M. M., Wallace, S. D., and Moe, K., "Recommended Drag Coefficients for Aeronomic Satellites," *Geophysical Monograph: Upper Mesosphere and Lower Thermosphere*, Vol. 87, 1995, pp. 349–445.

[22] Niven, W. D., *The Scientific Papers of James Clerk Maxwell*, Dover, New York, 1965.

[23] Goodman, F. O., "A Three-Dimensional Hard Spheres Theory of Scattering of Gas Atoms From a Solid Surface," NASA CR 933, 1967.

[24] Pilinski, M., Argrow, B., and Palo, S., "Semi-Empirical Model for Satellite Energy Accommodation Coefficients," *Journal of Spacecraft and Rockets*, 2010 (to be published).

[25] Picone, J. M., Hedin, A. E., and Drob, D. P., "NRLMSISE-00 Empirical Model of the Atmosphere: Statistical Comparisons and Scientific Issues," *Journal of Geophysical Research*, Vol. 107, No. A12, 2002, Paper 1468.
doi:10.1029/2002JA009430

[26] Doornbos, E., Forster, M., van Helleputte, T., van den Ijssel, J., Koppenwallner, G., Luhr, H., Rees, D., and Visser, P., "Air Density Models Derived from Multi-Satellite Drag Observations," European Space Agency TR 21022/07/NL/HE, 2009.

[27] Sutton, E., "Normalized Force Coefficients for Satellites with Elongated Shapes," *Journal of Spacecraft and Rockets*, Vol. 46, No. 1, 2009, pp. 112–116.
doi:10.2514/1.40940

[28] Drob, D. P., "An Empirical Model of the Earth's Horizontal Wind Fields: HWM07," *Journal of Geophysical Research*, Vol. 113, 2008, Paper A11319.
doi:10.1029/2008JA013668

[29] Bird, G. A., "Sophisticated DSMC," *DSMC07 Meeting*, Sept. 2007, http://www.gab.com.au/Resources/DSMC07notes.pdf [retrieved 31 Jan. 2010].

[30] Winters, H. F., Coufal, H., Rettner, C., and Bethune, D., "Energy Transfer From Rare Gases to Surfaces: Collisions With Gold and Platinum in the Range of 1–4000 eV," *Physical Review*, Vol. 41, No. 10, 1990, pp. 6240–6256.
doi:10.1103/PhysRevB.41.6240

[31] Doughty, R. O., and Schaetzle, W. J., "Experimental Determination of Momentum Accommodation Coefficients at Velocities up to and Exceeding Earth Escape Velocity," *Proceedings of the Sixth International Symposium on Rarefied Gas Dynamics*, edited by L. Trilling and H. Y. Wachman, Suppl. 5 , Vol. 2, Academic, New York, 1969, pp. 1035–1054.

[32] Reiter, G. S., and Moe, K., "Surface-Particle-Interaction Measurements Using Paddle-Wheel Satellites," *Rarefied Gas Dynamics*, edited by L. Trilling and H. Y. Wachman, Vol. 6, Academic Press, New York, 1968, pp. 1543–1554.

I. Boyd
Associate Editor